Volume 1 | Number 1 | Jan 2013 | Pages 1–100

Lab on a Chip

Miniaturisation for chemistry, physics, biology, materials science and bioengineering
www.rsc.org/loc

ROYAL SOCIETY OF CHEMISTRY

ROYAL SOCIETY OF CHEMISTRY

www.rsc.org/loc

Lab on a Chip

Lab on a Chip

Cite this: DOI: 10.1039/c0xx00000x

www.rsc.org/xxxxxx

PAPER

Compact microfluidic device for rapid concentration of PET tracers

Wei-Yu Tseng[a] and R. Michael van Dam[b]

Received (in XXX, XXX) Xth XXXXXXXXX 20XX, Accepted Xth XXXXXXXXX 20XX
DOI: 10.1039/b000000x

5 HPLC purification and reformulation of positron emission tomography (PET) tracers can lead to significant dilution of the final product, making it difficult to produce a sufficiently high radioactivity concentration for some applications (e.g. small animal imaging, *in vitro* assays, and labelling of proteins with prosthetic groups). This is especially true for molecules with lengthy or low-yield syntheses. Starting the synthesis with more radioactivity increases the final radioactivity concentration but increases hazards 10 and complexity of handling. An alternative is to concentrate the final product by a process such as rotary evaporation prior to downstream use. Because a rotovap requires significant space within a hot cell that could be put to more productive use, we developed a compact microfluidic system for concentration of PET tracers. This system also provides advantages in terms of repeatability, interfacing and potential for automation. We present here the design and performance characterization of the system, and demonstrate 15 the concentration of several tracers in aqueous-based HPLC mobile phases.

Introduction

Positron emission tomography (PET), especially with the radioisotope fluorine-18 (F-18), has become the key medical imaging modality for cancer diagnosis and treatment evaluation 20 [1,2] and is a powerful tool for *in vitro* and *in vivo* research in cancer biology [3,4] and drug development [5–7]. The PET tracers injected for imaging are produced manually or by automated radiosynthesizers housed in radiation-shielded fume hoods called "hot cells" to protect the operator from radiation exposure. As the 25 space inside these expensive hot cells is at a premium, there are significant efforts to miniaturize the equipment used in PET tracer production. In particular, several research groups are developing microfluidic chips for PET tracer synthesis, some coupled with purification, in answer to this challenge [8–14]. 30 However, miniaturization of the essential downstream processes of formulation and concentration have not been extensively studied (**Figure 1**).

Though the conventional synthesis of PET tracers is carried out in a relatively small reaction volume (~1 mL), a concentration step 35 is needed because the purification and formulation steps can significantly expand this initial volume, resulting in a final product for injection that is too dilute for use in many cancer research applications. For example, after purification by semi-preparative high-performance liquid chromatography (HPLC), a 40 volume of tens of mL is common. In cases where the HPLC mobile phase is not safe for injection, purification is followed by solid-phase extraction (SPE) to exchange the solvent. In the last stage of this process, the PET tracer is typically eluted from the cartridge with ethanol and then subsequently diluted with water 45 or saline (~10 mL) to reduce the ethanol content to acceptable levels [15].

On the other hand, existing and emerging platforms for *in vitro* cancer studies such as binding or uptake assays, drug response assays, enzyme activity assays, or kinetic modelling have 50 reported the need for concentrations up to ~1 mCi/mL [16], and *in vivo* imaging in mouse tumor models typically uses 200 μCi in a volume of 100 μL or less (limited by low blood volume of the mouse) which is a concentration of ~2 mCi/mL. Even higher concentrations of purified radiolabeled molecules are needed in 55 some applications. For example, prosthetic groups (e.g., N-succinimidyl-4-[18F]fluorobenzoate ([18F]SFB)) for labelling proteins must be produced in a high concentration after purification due to the small volume and relatively low yield of the labelling process[17]. 60 To achieve these concentrations when the final production volume is tens of mL, one can sometimes start with high levels of radioactivity. However, in cases where the laboratory is limited in the amount of radioactivity that can be used, or where the synthesis and purification processes are lengthy, the synthesis 65 yield is low (e.g., ~1% is typical for many tracers in the early evaluation and development stage), or the tracer must be delivered a long distance from the production site, it becomes necessary to perform a concentration step. The need for concentration is further exacerbated if the assays or imaging are 70 carried out over a long timespan.

It should be noted that although reaction volumes in microfluidic radiosynthesis platforms tend to be smaller than in conventional apparatus, the miniaturized purification approaches reported so far [13,18,19] tend still to result in significant dilution (to ~1-5 mL) 75 of tracers synthesized on-chip. In combination with the reduced

This journal is © The Royal Society of Chemistry 2014

Lab on a Chip Accepted Manuscript

production scale that is typical of these platforms, these miniaturized devices will similarly yield tracers that require concentration prior to *in vitro* or *in vivo* use.

Currently, concentration is achieved at rates of about ~1 mL/min
5 by a bulky rotary evaporator (rotovap) that occupies a large amount of real-estate inside the hot cell (or it may even require an additional hot cell). The large size of the rotovap increases the cost of tracer production by utilizing hot cell space that could otherwise be used to house additional radiosynthesizers for
10 increased tracer diversity. In addition, the lack of automation of liquid handling to and from the rotovap can result in radiation exposure to the operator and some transfer losses. It would therefore be advantageous to miniaturize and automate the concentration process.
15 The use of microfluidics for volume reduction has been explored by several groups [20–23]. The fastest approaches perform small scale membrane distillation [24], with the sample on one side of a porous membrane and a solvent removal process (condensation or gas flow) on the other. In the work of Xu *et al.* [22], perforated
20 sidewalls of the microchannel serve as the "membrane", and in the reports of Timmer *et al.* [21] and Sharma *et al.* [23], a larger surface area membrane layer is interposed between a sample channel and a gas flow channel. Continuous evaporation rates in the latter two reports were 0.006 mL/min and 1.8 mL/min,
25 respectively. In this paper, we demonstrate that microfluidic membrane distillation can be effectively be used as the basis for a system to concentrate PET tracers suspended in aqueous-based HPLC buffers (or buffers containing organic solvents provided that the contact angle on Teflon remains >90°) in a rapid,
30 convenient, and repeatable manner.

Methods

Concentrator Design

We designed and fabricated a microfluidic chip (**Figure 2**) based on the principle of the design reported by Sharma et al. [23]. In this
35 approach, a porous hydrophobic membrane separates the liquid sample from a stream of dry gas. The pores are sufficiently small that the aqueous sample cannot penetrate them at the applied pressure. However, vapor can be freely transported through the membrane. This vapor is driven by a difference in partial
40 pressures on the two sides of the membrane pores. On the sample side, the partial pressure is related to the temperature of the solvent; on the gas flow side, the partial pressure is kept low by an incoming stream of dry gas. Since solutes remain on the sample side of the membrane, the sample solution becomes more
45 concentrated.

The functional part of the chip consists of three layers: the sample layer, the membrane, and the gas flow layer. The sample layer was made from a 2mm thick acrylic plate patterned with a serpentine channel (4.5 mm wide x 170 μm deep; 0.5 mm
50 spacing) and was fabricated by ALine, Inc. (Rancho Dominguez, CA). Acrylic is chemically compatible with the aqueous solutions to be concentrated and its transparency facilitates visual monitoring of the concentration process. The volume of this channel is 1.0 mL and the surface area of liquid in contact with
55 the membrane is 5800 mm². The gas flow layer consists of a 1 cm thick block of aluminium with an identical channel (except depth

is 2mm) patterned in the surface via CNC machining (Proto Labs, Inc., Maple Plain, MN). A 100W cartridge heater (8376T27, McMaster Carr) and temperature sensor (K type thermocouple,
60 OMEGA Engineering, Inc., Stamford, CT) were inserted into holes drilled into the gas flow layer and connected to a temperature controller (CN7500, OMEGA Engineering, Inc., Stamford, CT). Heat is transferred through the membrane to the sample layer to heat the sample solution. Since the heating does
65 not occur directly in the sample layer, we expect a small difference in temperature of the sample layer and the actively-controlled gas flow layer.

The heater capacity was selected based on the following calculation. The estimated heat energy needed to heat a 10 mL
70 sample of water from 20°C to 100°C, and then convert this into the vapour phase is ~26 kJ. Our ultimate aim is to achieve the evaporation within 10 min; thus the corresponding power required is 43 W. Since there will be other heat losses, and electrical power consumption is not a limitation in this
75 application, we opted for a 100W heater to ensure the temperature of the chip could be maintained throughout the sample concentration process.

A membrane layer was sandwiched between the sample and gas flow layers. Two different membranes were considered: a
80 Zeflour membrane with 1 μm pore size (Pall Life Sciences, Port Washington, NY, USA) and a PTFE membrane with 1 μm pores (Sterlitech, Kent, WA, USA). An additional 2.4 cm thick acrylic plate is placed on top of the sandwich to provide structural rigidity for clamping all of the layers together using screws.
85 Because the layers are not individually bonded together, it is necessary that the channel patterns in the sample and gas flow layers be identical and aligned.

A reservoir containing the sample was connected to the inlet of the sample layer of the chip via tubing (1/16" OD, 0.03" ID,
90 Teflon PFA, Idex Health & Science, Oak Harbor, WA). The sample reservoir was also connected to a regulated source of inert gas (nitrogen). The outlet of the sample layer was connected to a valve and then to a collection reservoir. A regulated inert gas source (nitrogen) was connected to the inlet of the gas flow layer
95 and a vacuum trap and vacuum pump were connected to the outlet of the gas flow layer. Pressure gauges close to the chip were used to monitor the inlet (P_{gas_in}) and outlet (P_{gas_out}) pressures. Pressures were controlled with electro-pneumatic regulator (ITV0010 and ITV2010, SMC Pneumatics, Yorba
100 Linda, CA, USA) and electronic vacuum regulators (ITV2090, SMC Pneumatics, Yorba Linda, CA, USA) connected via a data acquisition module (NI USB-6009, National Instruments, Austin, TX, USA) to a computer running a custom program written in Labview.

105 ### Concentrator Operation

Samples were concentrated via the steps in **Figure 3**. The chip is first preheated until it stabilizes at the desired operating temperature. With our current heater, this took ~15min, but could be performed in parallel with the synthesis of the PET tracer so
110 that the microfluidic concentrator is ready to be used immediately at the end of synthesis. Next, the outlet valve is closed and the sample is delivered into the chip by applying gas pressure P_{sample} to the sample reservoir. The air ahead of the liquid (i.e. in the tubing and the chip) rapidly escapes through the membrane

allowing the sample channel of the chip to be quickly filled with liquid (~15 s). Next, the gas flow is applied by setting P_{gas_in} and P_{gas_out} by tuning the regulators to achieve the desired pressure readouts on the gauges, and the evaporation is carried out. The
5 constant application of P_{sample} to the sample reservoir ensures that new liquid is delivered to the chip to replace the solvent being evaporated. When nearly the entire solvent volume has been evaporated (i.e. sample reservoir and tubing are empty and sample is only present within the chip), the sample outlet valve is
10 opened, and a vacuum (pressure V) is applied to the collection vial (with P_{sample} and gas flow still applied) to recover the sample solution. If only pressure or vacuum was applied independently during collection, we observed the liquid to become fragmented, resulting in significant liquid residue remaining in the channel.

15 **Performance Evaluation**

The performance of the concentration process was quantified by comparing starting and ending volumes using graduated markings on the sample and collection vials, and by determining the fraction of the initial amount of solute that is collected in the final
20 concentrated output. The latter was determined using samples of ^{18}F-labeled PET tracers and comparing radioactivity of the starting and ending vials and correcting for radioactive decay of fluorine-18 (110 min half-life). Radioactivity measurements were made using a calibrated dose calibrator (CRC-25 PET, Capintec,
25 Inc., Ramsey, NJ).

Determination of operating parameters

The ability of the membrane to prevent the liquid sample from directly flowing through it is primarily based on the contact angle, θ, of the liquid on the membrane material. For θ < 90°,
30 capillary force causes the liquid to spontaneously flow through the membrane. On the other hand, if θ > 90°, then the capillary force opposes flow through the membrane, and liquid can only enter the membrane if driven by a pressure exceeding the capillary pressure,
35

$$p_c = \frac{2\gamma \cos\theta}{r}$$

where γ is the surface tension of the liquid, and r is the pore radius. Commercial membranes are typically characterized by a related quantity called the liquid entry pressure (P_{LEP}), determined empirically due to the distribution of different pore
40 sizes in commercial membranes [25,26].
In addition to membrane material, contact angle depends on composition of the liquid and temperature. Because the concentration of PET tracers involves HPLC mobile phases (buffers) that are typically not pure solvents and temperatures that
45 are significantly above room temperature, membrane performance under these conditions is not generally available from manufacturers and thus P_{LEP} was determined empirically. Food dye was added to the sample (~1% v/v) to enhance visibility. The chip was preheated to the desired temperature.
50 Next the sample was loaded into the chip. The applied pressure P_{sample} was gradually increased (in increments of 0.5 psig) until dye was observed in the gas flow channel (i.e., evidence that the liquid had directly penetrated the membrane). P_{gas_in} and P_{gas_out} were maintained at 0 psig throughout the experiment. The P_{LEP}

55 was critical in determining optimal operating pressures for a given combination of HPLC buffer composition and operating temperature.

Determination of Evaporation Rate

Evaporation rate was monitored by placing markings along the
60 length of transparent tubing between the sample reservoir and the chip at 1 mL intervals. For these studies, the tubing length was chosen such that its internal volume was larger than the total sample to be concentrated. Upon pressurization of the sample reservoir, the sample fills the tubing and chip, and the progression
65 of the trailing meniscus through the tubing can be monitored during the evaporation process. The evaporation rate was determined from the elapsed time between the meniscus reaching the desired start and end markings. No dye was needed to monitor the evaporation rate.

70 **Determination of Solvent Content**

Ethanol content of samples was measured using a gas chromatograph (GC; Agilent 7890A) equipped with a mass spectroscopy detector, an auto sampler and a JW DB-WAX (polyethylene glycol) column (30 m long, 0.25 mm ID and a
75 phase thickness of 0.25 μm) using a previously developed method[27]. The GC was operated with a helium flow of 1.5 mL/min. The initial oven temperature was set at 35°C and held for 2 min followed by a temperature ramp of 10°C/min to 80°C. After holding at 80°C for 0.5 minute, the temperature was ramped
80 at 10°C/min to 150°C and held for 10 minutes to separate the solvents. A calibration curve was generated from known samples prior to quantitation of ethanol in unknown samples.

Reagents

Food dye was purchased from Kroger (USA) and was diluted
85 1:100 with 18MΩ deionized water. Ethanol (200 proof) was purchased from the UCLA Chemistry Department (Los Angeles, CA, USA). Ammonium dihydrogen phosphate ($NH_4H_2PO_4$), anhydrous grade acetonitrile (MeCN) and trifluoroacetic acid (TFA) was purchased from Sigma-Aldrich (Milwaukee, WI
90 USA).
1-(2'-deoxy-2'-[18]fluoroarabinofuranosyl) cytosine ([^{18}F]FAC) was synthesized and purified using the ELIXYS radiosynthesizer [28] and used directly with the concentrator chip. The purified tracer was already dissolved in the HPLC mobile phase for
95 [^{18}F]FAC (see **Table 1**). Due to the limited availability of [^{18}F]FAC, we performed some experiments using 2-[18]fluoro-2-deoxy-D-glucose ([^{18}F]FDG) dissolved in the same mobile phase. [^{18}F]FDG in saline was obtained from the UCLA Biomedical Cyclotron facility, and several 100 μL portions (containing ~100
100 μCi) were each dissolved into 10 mL mobile phase. We expect the evaporation performance to be determined by the mobile phase and not the particular tracer used.
We also investigated the concentration of the prosthetic group N-succinimidyl-4-[18]fluorobenzoate ([^{18}F]SFB) which is purified
105 using an HPLC buffer with high solvent content (50:50 MeCN/water; see **Table 1**). [^{18}F]SFB was synthesised using the ELIXYS radiosynthesizer [29]. Due to the high amount of organic solvent in the purified sample, the solution has contact angle <90° on Teflon and thus spontaneously flows through the membrane.
110 Therefore, prior to loading into the concentrator chip, [^{18}F]SFB

was exchanged to an aqueous solution through a solid-phase extraction process. To minimize radiation exposure, only a 1 mL portion (containing ~1 mCi) of the purified [18F]SFB solution was used; it was diluted with 9 mL of water, and flowed through a C-
5 18 cartridge (WAT023501, Waters, Milford, MA, USA) to trap the [18F]SFB, followed by drying with nitrogen. (Normally, the entire volume would be diluted ~1:10 with water and trapped on the same cartridge.) The [18F]SFB was eluted with 1 mL ethanol and then several 100 μL portions (containing ~100 μCi) were
10 each diluted to 10 mL to create samples to be concentrated by the chip. If used for peptide- or protein-labelling purposes, the dilution would be performed with a buffer compatible with labelling, but we diluted with the mobile phase for [18F]FAC to ensure that evaporation rates of different experiments could be
15 compared.

Results and Discussion

Optimization of operating conditions

Due to the importance of minimizing time in the production of PET tracers, we first explored the operating limits of the
20 microfluidic concentrator to maximize the evaporation rate. The evaporation rate is determined by several factors: temperature, surface area of sample solution exposed to the membrane, membrane pore size and density, and gas flow rate in the bottom channel layer.
25 Evaporation rate is expected to increase linearly with surface area. In the design of the chip, we have tried to maximize the surface area by designing a serpentine channel that uses most of the available surface area of the chip. Chips larger than the current size quickly become impractical; thus we consider the
30 current size to be an upper limit. It is possible that a stacking approach with multiple membrane layers to achieve a significantly higher surface area may be a promising direction for further optimization in the future.

Several membranes were initially considered, including (i) 1μm
35 pore size Zefluor™ membrane (0.0073" total thickness, including PTFE support layer, Pall Science, USA), (ii) 0.2 μm pore size PTFE membrane (0.0013" total thickness, Sterlitech, USA), (iii) 1 μm pore size PTFE membrane (0.0081" total thickness, Sterlitech, USA), and (iv) 0.45 μm pore size PTFE (0.0043" total
40 thickness, including polypropylene support layer, Sterlitech, USA). Each membrane was first installed individually into the chip and the assembled chip was tested for leakage between the membrane and sample channel by filling it with water. We found that the 0.45 μm pore membrane consistently leaked, presumably
45 due to the texture of the support layer that prevented proper sealing between the sample layer and the membrane. The 0.2 μm pore size membrane did not leak, but due to the thinness of the membrane, it underwent significant deformation at modest pressures, tending to block the gas flow channel and thereby
50 reducing evaporation rate significantly. Neither of these membranes was used in further experiments, but it may be possible to overcome mechanical limitations of the latter membrane by reducing the channel width or combining the membrane with a more rigid backing layer.
55 We next considered the effect of adjustable parameters on the evaporation performance.

Temperature

The maximum operating temperature of the device itself is around 110 °C, limited by the glass transition temperature of the
60 acrylic material, above which significant deformation will disrupt the integrity of the seal between the layers. Another concern is thermal degradation of the PET tracer being concentrated. Since rotary evaporation of PET tracers is commonly performed at temperatures in the range 50 to 100°C, we limited our
65 investigation to 100°C. Another constraint on temperature is the reduction of contact angle (and thus the liquid entry pressure of the membrane, P_{LEP}) at increasing temperature. If the contact angle drops to 90° or less, the membrane will no longer act as a barrier and the liquid sample will spontaneously flow through it
70 (i.e. P_{LEP} will drop to zero or less). We first empirically evaluated P_{LEP} of water for each membrane as a function of temperature to determine at what point the P_{LEP} becomes too low to be practical. For chip temperatures of 50, 60, 70, and 80°C, P_{LEP} was found to be in the range 4.0 – 4.5 psig for the 1μm pore size Zefluor
75 membrane and 2.0 – 2.5 psig for the 1 μm pore size PTFE membrane. For chip temperatures of 90 and 100 °C, P_{LEP} was found to be 3.5 – 4.0 psig and 1.5 – 2.0 psig for the two membranes, respectively. The [18F]FAC HPLC mobile phase (**Table 1**) contains a small amount (1%) of ethanol. Though
80 mixtures of water with organic solvents in general have lower contact angle on Teflon (compared to pure water), similar P_{LEP} were obtained using the HPLC mobile phase as were obtained for water.

The vapour pressure of the solvent is exponentially related to
85 temperature, and by making some simple assumptions, one would expect the evaporation rate to vary exponentially with temperature. **Figure 4a** shows the measured evaporation rate (of water) as a function of temperature. An exponential fit exhibits R^2 >0.99. These results clearly suggest that the highest
90 evaporation rate will be achieved by maximizing the temperature.

Sample Composition

Since most organic solvents have a contact angle <90° on most materials (including Teflon), the concentrator is most suitable for aqueous samples. However, studies have shown that the contact
95 angle on Teflon remains >90° up until as high as 75 % EtOH in water at 40°C [25,30]. At a chip temperature of 80°C, where the evaporation rate is significantly higher, we found empirically that proportions of organic solvents up to ~20% EtOH or ~15% MeCN in water could be used (i.e. $P_{LEP} > 1$ psi) in conjunction
100 with the 1 μm pore PTFE membrane. This tolerance of organic solvents provides considerable flexibility to concentrate PET tracers purified with a diverse range of mobile phases. For mobile phases with greater organic solvent content and/or containing highly toxic organic solvents (e.g. MeCN), it may be necessary to
105 first exchange the solvent to EtOH via a cartridge method and then dilute with water to reduce the ethanol content below allowed injection limits prior to microfluidic concentration.

Because acrylic is not particularly resistant to organic solvents, its use in the concentrator may also restrict the type and amount of
110 organic solvents that can be tolerated. If necessary, this limitation could be addressed in future work by the use of a more inert polymer for construction of the sample layer of the device.

Gas Flow

The flow rate through the gas channel depends on the channel geometry and is related linearly to the pressure difference P_{gas_out} − P_{gas_in}, where $P_{gas\_in} > P_{gas\_out}$. It is expected that a higher gas flow rate would more rapidly remove vapour from the device and thereby maintain a lower partial pressure of the solvent on the gas flow side of the membrane, increasing the rate of solvent removal.

The interaction with other pressures in the system via the membrane imposes some limitations on the values of P_{gas_in} and P_{gas_out}. If we assume that the solvent evaporates sufficiently slowly that the flow of fresh sample into the chip is very slow, then to a good approximation, the liquid on the sample side of the membrane would be at a constant and uniform pressure P_{sample}. To avoid air flow through the membrane, into the sample channel, and pushing of the sample out of the chip toward the reservoir, it is necessary that no pressure in the gas flow layer exceed P_{sample}; i.e. $P_{gas\_in} < P_{sample}$. To prevent liquid flow through the membrane from the sample channel to the gas flow channel, it is necessary that maximum pressure across the membrane, P_{sample} − $P_{gas\_out} < P_{LEP}$. These constraints taken together imply that the gas flow pressure differential, $P_{gas\_in} − P_{gas\_out} < P_{LEP}$. Within these operating limits, we evaluated the effect of this pressure difference on the evaporation rate (**Figure 4b**) and found a small increase in evaporation rate with higher pressure difference. We thus elected to use the maximum possible pressure differential in subsequent experiments.

Dynamics of evaporation rate

The boiling point of a solvent is generally elevated by the addition of solutes according to the relation $\Delta T = K_b m$, where K_b is a constant characteristic of the solvent, and m is the molality of the solvent. As the solution inside the sample layer of the chip becomes more concentrated, it is possible that its boiling point increases and that the rate of evaporation decreases. Complicating this effect is the non-uniform concentration distribution within the sample channel (generated because fresh sample is always loaded from one end) that may result in varying evaporation rate along different parts of the sample channel. It is also possible that evaporation rate could be affected over time by membrane fouling or other factors [24].

In addition, if the sample consists of a solvent mixture, its composition may shift during the concentration process toward a mixture richer in the higher boiling solvent, thus reducing the evaporation rate. Using gas chromatography, we observed the ethanol content of the [18F]FAC mobile phase to be significantly decreased (down to ~10-15% of the initial value) after concentration. For the same volume evaporated, higher temperature was found to cause greater reduction of ethanol (data not shown).To investigate whether these are important effects with respect to evaporation rate, we empirically monitored the evaporation rate as a function of the solvent volume evaporated (and thus the concentration of solutes). **Figure 5** shows the evaporation rate for each 1.0 mL increment of liquid evaporated. Results were compared for water and for the sample of [18F]FAC HPLC mobile phase (**Table 1**). For a 1.0 mL chip volume, the x-axis can also be interpreted as the fold-increase in the average concentration of the sample that is contained within the chip. The results show a very minor decrease in evaporation rate as a function of concentration. However, we expect a larger effect

would be observed for HPLC mobile phase solution when the initial volume is large (e.g. 20mL or 50mL).

Demonstration of sample concentration

After optimization of operating conditions, we concentrated 10.0 mL batches of water mixed with food dye at 80°C. The overall time to collect the final sample was 20.8 min. The final volume was 1.25 ± 0.05 mL (n=2), slightly larger than the expected volume of 1.0 mL, presumably due to slight outward deformation of the membrane, which allowed more volume to occupy the channel. The evaporation rate was 0.421 ± 0.025 mL/min (n=2). We also used the chip to concentrate samples of purified [18F]FAC. The chip was pre-heated to 80°C and a 9.0 mL [18F]FAC sample was loaded in the sample reservoir and delivered to the chip. Evaporation was continued until the volume was reduced to 90% of the channel volume. The average volume collected was 0.90 ± 0.05 mL (n=2), the average evaporation rate was 0.434 ± 0.034 mL/min (n=2) and the average overall processing time was 18.6 min. In these two experiments, the amount of radioactivity recovered was 74% and 82% of the initial radioactivity (corrected for decay).

The evaporation rate for these samples was lower than our target of 1.0 mL/min, but the compact size, easy integration, and potential for full automation (currently underway) represent significant advantages over the approach of rotary evaporation.

Optimization of sample recovery

We hypothesized that the majority of the losses of radioactivity were due to liquid residue left in the chip and tubing after the sample was collected from the chip. To further increase the radioactivity recovered, we employed a strategy of rinsing the chip with multiple small volume plugs of HPLC mobile phase. Since doing so has an adverse effect on concentration (i.e. increases the final volume) and time (i.e. lengthens the concentration process), we investigated the radioactivity recovery as a function of the number of rinses to find the lowest number of rinses that would improve the recovery. For 80°C evaporation, a rinse volume of 500 μL was chosen. Because the chip is still at elevated temperature during rinsing, the plug shrunk to a volume of ~250 μL by the time it exited the chip and was collected. Rinse plugs were loaded into the sample vial and propelled through the chip by applying pressure P_{sample} to the sample vial and vacuum pressure V to the collection vial simultaneously. Each rinse step took ~3 min.

Using a sample of [18F]FDG diluted in 10 mL of 1:99 EtOH/10mM $NH_4H_2PO_4$ v/v), we experimentally investigated the effect of multiple rinse steps. The amount of radioactivity in the collection vial was measured after the initial sample recovery and after each of four consecutive rinse steps. In three experiments, increasing the number of rinse plugs showed improved recovery of radioactivity, but there was negligible improvement beyond the first two plugs (**Figure 6**). At a temperature of 80°C, the average evaporation rate was 0.443 ± 0.011 mL/min (n=3). The average recovery of the radioactivity was initially 83±4% (n=3), and increased to 89±3% (n=3) after two rinse plugs, representing a 7% increase (corrected for radioactive decay) in recovered PET tracer. If we account for the amount of tracer lost to radioactive decay over the ~6 min rinse time, then we still obtain a 3% increase (non-corrected) in overall recovery.

After each experiment, flushing with 10 mL of liquid was able to recover the majority of the remaining radioactivity suggesting that the residual amount may result from dead volumes within the channel or completely dried residues that cannot be quickly
5 redissolved, rather than from some physical adsorption process that renders the PET tracer unrecoverable. We suspect that improved channel design (e.g. avoiding sharp corners) will improve the recovery attainable with this chip. It is possible that other PET tracers will strongly adsorb to the acrylic material and
10 in these cases, alternate materials can be considered for construction of the sample layer of the chip.

Optimized performance

We next combined optimized solvent removal (at a temperature of 100°C) with the optimized concentrated sample recovery
15 process. A sample of [^{18}F]SFB in 10 mL of 1:99 EtOH/10mM NH$_4$H$_2$PO$_4$ (v/v) was concentrated. Using the 1 μm pore size PTFE membrane and pressures P$_{sample}$ = P$_{gas\_in}$= 1.5 psig; P$_{gas\_out}$ = 0.0 psig, we observed an average evaporation rate of 0.658 ± 0.004 mL/min (n=3) and an overall radioactivity recovery of 93 ±
20 2% (n=3) after concentration followed by two rinse steps. The final volume was 1.82 ± 0.15 mL (n=3). We plan to investigate in future work a lower volume chip design that we anticipate could achieve smaller volume after sample recovery. Analytical radio-HPLC analysis of [^{18}F]SFB samples before and after
25 concentration suggest that no thermal or radiolytic decomposition occurred during the concentration process. Although we did not encounter issues for this probe, it is still important to study thermal decomposition before using the concentrator to concentrate other probes.

30 **Comparison with rotary evaporation**

Use of the microfluidic concentrator has several advantages compared to rotary evaporation. One of these is size. Rotary evaporators are large laboratory instruments: to the best of our knowledge, the custom-built rotovap system [31] at our institute (17
35 cm x 36 cm x 24 cm) is smaller than any remotely-controllable commercial system. Typically the rotary evaporator must be housed in a commercial hot cell or mini cell to provide sufficient radiation shielding of the evaporator during operation. This encroaches on valuable hot cell real estate in a radiochemistry
40 lab, in which installation of another radiosynthesizer would be preferred. The dimensions of the microfluidic concentrator that require radiation shielding, on the other hand, are only 13 cm x 13 cm x 4 cm (about 5% of the rotovap size), allowing the system to easily be placed and operated on top of, beside, or behind the
45 synthesizer. It is even conceivable that customized shielding could be constructed and the concentrator system operated outside a hot cell or mini cell (e.g. in conjunction with a hypothetical microfluidic-based benchtop synthesizer). The performance of the microfluidic system was also found to be
50 very repeatable. Evaporation rates exhibited 2.5% variation during concentration of [^{18}F]FDG samples at 80°C (n=3) and 0.6% variation during concentration of [^{18}F]SFB samples at 100°C (n=3). In addition, the microfluidic system is also straightforward to
55 integrate with many existing synthesizers and purification systems simply by replacing the normal collection vial with the sample reservoir of the concentrator, and then connecting the

collection vial to the concentrator output.
The microfluidic system also has a high potential for automation.
60 Rotary evaporation often requires many manual (but remotely-controlled) steps to load the sample, monitor the process, and collect the concentrated product. We are developing system-level automation for the microfluidic concentrator to enable reliable completion of the entire concentration process without user
65 intervention. We plan to investigate the possibility of developing electrical interfaces to enable the concentration process to be initiated from the existing software of several commercial radiosynthesizers.

Conclusions

70 We designed and tested a compact microfluidic concentrator to concentrate batches of PET tracers in aqueous-based media prior to preclinical imaging, to enable HPLC-purified tracers to have sufficient concentration for *in vivo* and *in vitro* studies. The concentration of prosthetic radiolabeling agents can also be
75 increased by this device for improved coupling with proteins. Occupying only a tiny fraction the space of a conventional rotary evaporator, the microfluidic concentrator could still achieve good solvent removal performance. Furthermore the evaporation rate was very repeatable. In one demonstration, a mobile phase
80 containing 1% (v/v) EtOH was evaporated at a rate of 0.658 ± 0.004 mL/min (n=3), compared to a typical rate of 1.0 mL/min for rotary evaporation. We studied the adjustable parameters (temperature, pressures, and gas flow) to find the optimal evaporation conditions in the
85 current chip design and successfully concentrated samples of three PET tracers on-chip. Of all the parameters tested, temperature had the largest impact. Recovery of the dissolved species was improved by rinsing the channel with small volumes of HPLC mobile phase after initial collection from the chip.
90 Under optimized conditions, [^{18}F]SFB (as an example molecule) was concentrated from 10mL to 1.82mL in ~19 min at 100°C, and 93 ± 2% (n=3) of the radioactivity (decay-corrected) was collected. Future studies will focus on design improvements to increase evaporation rate and to reduce the need for time-
95 consuming rinse steps, as well as system-level improvements to enable fully-automated operation.
   Besides concentration of the PET tracers after HPLC purification, the concentrator could also be used in other applications. For example, over time, the concentration of Ga-68
100 eluted from a generator becomes progressively more dilute and difficult to use in the downstream synthesis. The concentrator could be used to reduce the volume of the eluted radioisotope to the typical volumes used in automated radiosynthesizers (0.4-1 mL) [32].

Notes and references

[a] *Crump Institute for Molecular Imaging and Department of Molecular & Medical Pharmacology, University of California, Los Angeles, 570 Westwood Plaza, Los Angeles, CA, 90095; Tel:310-206-6507; E-mail: wytseng@mednet.ucla.edu*
[b] *Crump Institute for Molecular Imaging and Department of Molecular & Medical Pharmacology, University of California, Los Angeles, 570 Westwood Plaza, Los Angeles, CA, 90095; Tel:310-206-6507; E-mail: mvandam@mednet.ucla.edu*

1. M. E. Phelps, *Proc. Natl. Acad. Sci. U. S. A.*, 2000, **97**, 9226 –9233.
2. W. A. Weber, *J Nucl Med*, 2005, **46**, 983–995.
3. V. Ambrosini, C. Quarta, C. Nanni, C. Pettinato, R. Franchi, G. Grassetto, A. Al-Nahhas, S. Fanti, and D. Rubello, *Cancer Biother. Radiopharm.*, 2009, **24**, 277–285.
4. M. Honer, M. Brühlmeier, I. Novak-Hofer, and S. Ametamey, in *PET and PET-CT in Oncology*, Springer Berlin Heidelberg, 2004, pp. 77–85.
5. M. Bergström, A. Grahnén, and B. Långström, *Eur. J. Clin. Pharmacol.*, 2003, **59**, 357–366.
6. W. A. Weber, *J. Clin. Oncol.*, 2006, **24**, 3282–3292.
7. M. T. Klimas, *Mol. Imaging Biol.*, 2002, **4**, 311–337.
8. C.-C. Lee, G. Sui, A. Elizarov, C. J. Shu, Y.-S. Shin, A. N. Dooley, J. Huang, A. Daridon, P. Wyatt, D. Stout, H. C. Kolb, O. N. Witte, N. Satyamurthy, J. R. Heath, M. E. Phelps, S. R. Quake, and H.-R. Tseng, *Science*, 2005, **310**, 1793–1796.
9. J. M. Gillies, C. Prenant, G. N. Chimon, G. J. Smethurst, W. Perrie, I. Hamblett, B. Dekker, and J. Zweit, *Appl. Radiat. Isot.*, 2006, **64**, 325–332.
10. J. M. Gillies, C. Prenant, G. N. Chimon, G. J. Smethurst, B. A. Dekker, and J. Zweit, *Appl. Radiat. Isot.*, 2006, **64**, 333–336.
11. C. J. Steel, A. T. O'Brien, S. K. Luthra, and F. Brady, *J. Label. Compd. Radiopharm.*, 2007, **50**, 308–311.
12. A. M. Elizarov, R. M. van Dam, Y. S. Shin, H. C. Kolb, H. C. Padgett, D. Stout, J. Shu, J. Huang, A. Daridon, and J. R. Heath, *J Nucl Med*, 2010, **51**, 282–287.
13. P. Y. Keng, S. Chen, H. Ding, S. Sadeghi, G. J. Shah, A. Dooraghi, M. E. Phelps, N. Satyamurthy, A. F. Chatziioannou, C.-J. Kim, and R. M. van Dam, *Proc. Natl. Acad. Sci.*, 2012, **109**, 690–695.
14. R. Bejot, A. M. Elizarov, E. Ball, J. Zhang, R. Miraghaie, H. C. Kolb, and V. Gouverneur, *J. Label. Compd. Radiopharm.*, 2011, **54**, 117–122.
15. X. Shao, R. Hoareau, A. C. Runkle, L. J. M. Tluczek, B. G. Hockley, B. D. Henderson, and P. J. H. Scott, *J. Label. Compd. Radiopharm.*, 2011, **54**, 819–838.
16. N. T. Vu, Z. T. F. Yu, B. Comin-Anduix, J. N. Søndergaard, R. W. Silverman, C. Y. N. Chang, A. Ribas, H.-R. Tseng, and A. F. Chatziioannou, *J. Nucl. Med.*, 2011, **52**, 815 –821.
17. T. Olafsen, S. J. Sirk, S. Olma, C. K.-F. Shen, and A. M. Wu, *Tumor Biol.*, 2012, **33**, 669–677.
18. M. D. Tarn, G. Pascali, F. De Leonardis, P. Watts, P. A. Salvadori, and N. Pamme, *J. Chromatogr. A*, 2013, **1280**, 117–121.
19. G. J. Shah, J. Lei, S. Chen, C.-J. 'CJ' Kim, P. Y. Keng, and R. M. Van Dam, in *Proceedings of the 16th International Conference on Miniaturized Systems for Chemistry and Life Sciences*, Royal Society of Chemistry, Okinawa, Japan, 2012, pp. 356–358.
20. G. M. Walker and D. J. Beebe, *Lab. Chip*, 2002, **2**, 57.
21. B. H. Timmer, K. M. van Delft, W. Olthuis, P. Bergveld, and A. van den Berg, *Sens. Actuators B Chem.*, 2003, **91**, 342–346.
22. W. Xu, L. L. Wu, G. P. Li, and M. Bachman, in *Proceedings of the Fourteenth International Conference on Miniaturized Systems for Chemistry and Life Sciences*, Groningen, The Netherlands, 2010, pp. 1208–1210.
23. N. R. Sharma, A. Lukyanov, R. L. Bardell, L. Seifried, and M. Shen, in *Microfluidics, BioMEMS, and Medical Microsystems VI*, eds. W. Wang and C. Vauchier, SPIE, San Jose, CA, USA, 2008, vol. 6886, p. 68860R–9.
24. M. S. El-Bourawi, Z. Ding, R. Ma, and M. Khayet, *J. Membr. Sci.*, 2006, **285**, 4–29.
25. M. C. García-Payo, M. A. Izquierdo-Gil, and C. Fernández-Pineda, *J. Colloid Interface Sci.*, 2000, **230**, 420–431.
26. C. Adiche and K. Sundmacher, *Chem. Eng. Process. Process Intensif.*, 2010, **49**, 425–434.
27. M. R. Javed, S. Chen, H.-K. Kim, L. Wei, J. Czernin, C.-J. 'CJ' Kim, R. M. van Dam, and P. Y. Keng, *J. Nucl. Med.*, 2014, **55**, 321–328.
28. H. Herman, G. Flores, K. Quinn, M. Eddings, S. Olma, M. D. Moore, H. Ding, K. P. Bobinski, M. Wang, D. Williams, D. Wiliams, C. K.-F. Shen, M. E. Phelps, and R. M. van Dam, *Appl. Radiat. Isot.*, 2013, **78**, 113–124.
29. M. Lazari, B. Maraglia, J. Collins, D. Yeh, M. Moore, and R. M. Van Dam, 2013, Unpublished manuscript.
30. V. Y. Dindore, D. W. F. Brilman, F. H. Geuzebroek, and G. F. Versteeg, *Sep. Purif. Technol.*, 2004, **40**, 133–145.
31. B. Amarasekera, P. D. Marchis, K. P. Bobinski, C. G. Radu, J. Czernin, J. R. Barrio, and R. M. van Dam, *Appl. Radiat. Isot.*, 2013, **78**, 88–101.
32. D. Mueller, I. Klette, R. P. Baum, M. Gottschaldt, M. K. Schultz, and W. A. P. Breeman, *Bioconjug. Chem.*, 2012, **23**, 1712–1717.
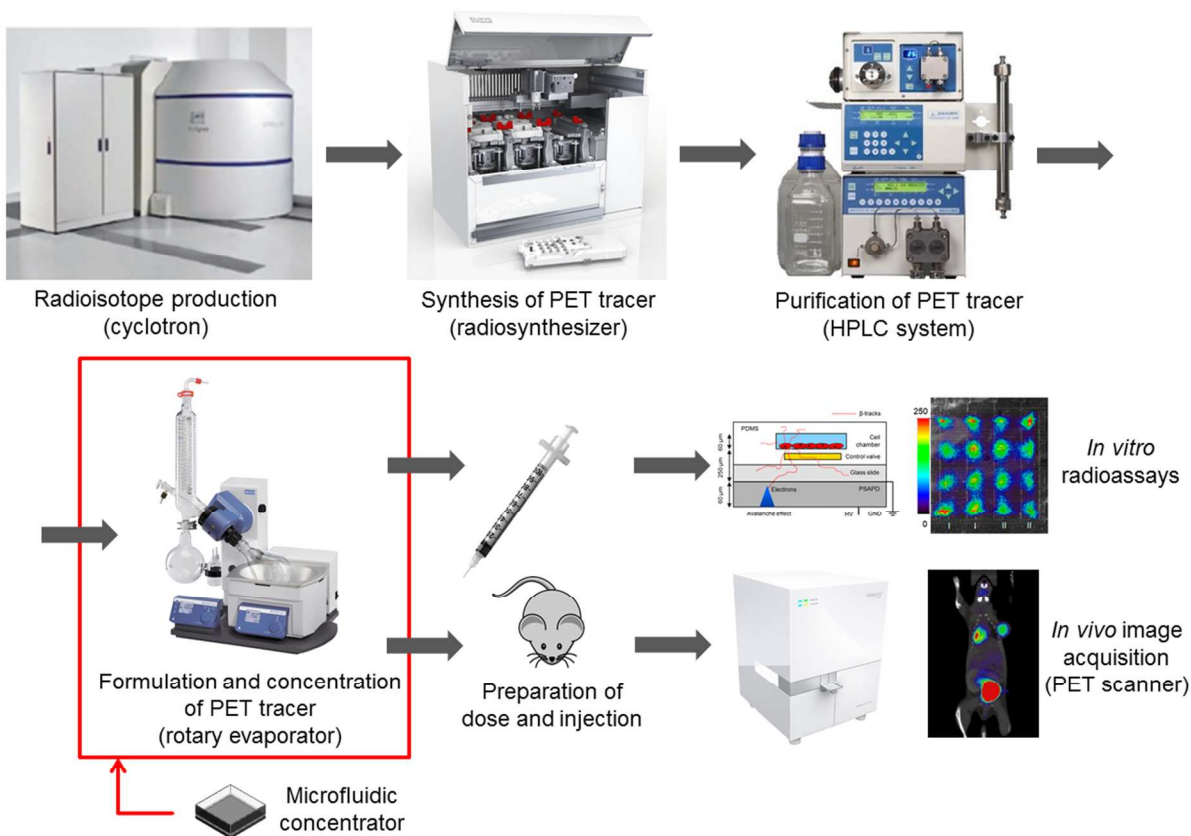
Lab on a Chip Accepted Manuscript

Figure 1. Typical workflow of PET tracer production and preclinical applications. This paper focuses on miniaturization of the outlined step.
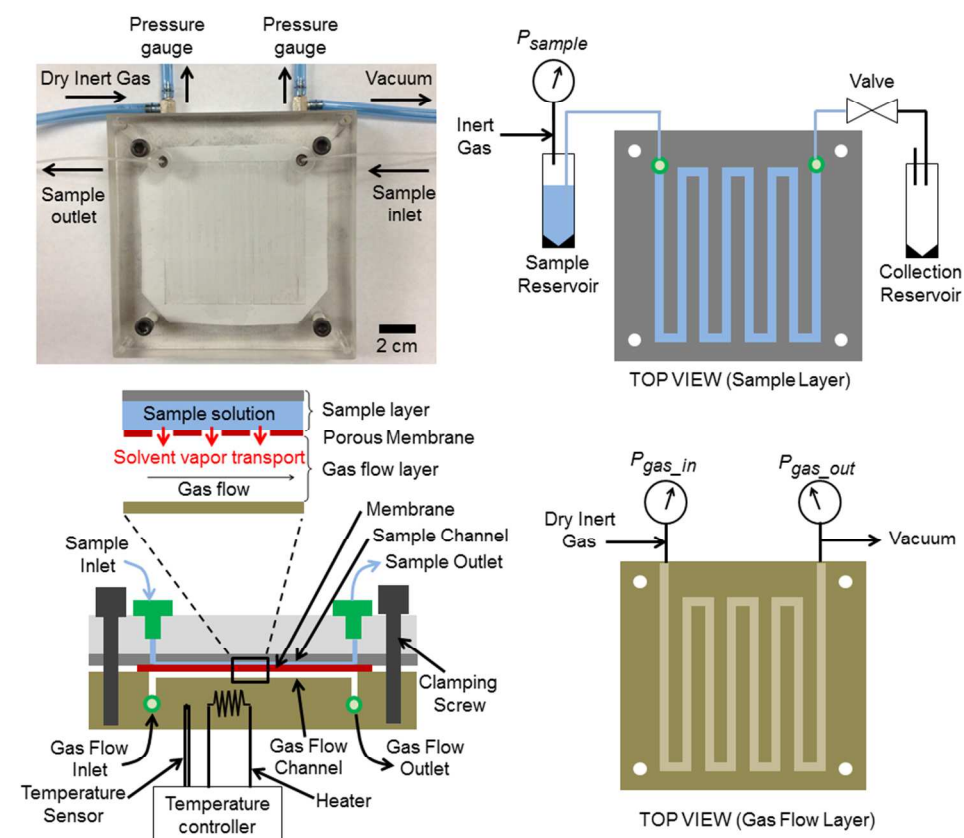
Figure 2. Top Left: Photograph of the microfluidic concentrator. Bottom Left: Schematic cross-section of the microfluidic concentrator. The inset illustrates the operating principle of vapor transport through the membrane. Top Right: Channel pattern in the sample layer of the chip, including connections to other system components. Bottom Right: Channel pattern and connections for the gas flow layer of the chip. The number of passes of the serpentine channel illustrated in these schematics is reduced (compared to the actual device) for clarity.
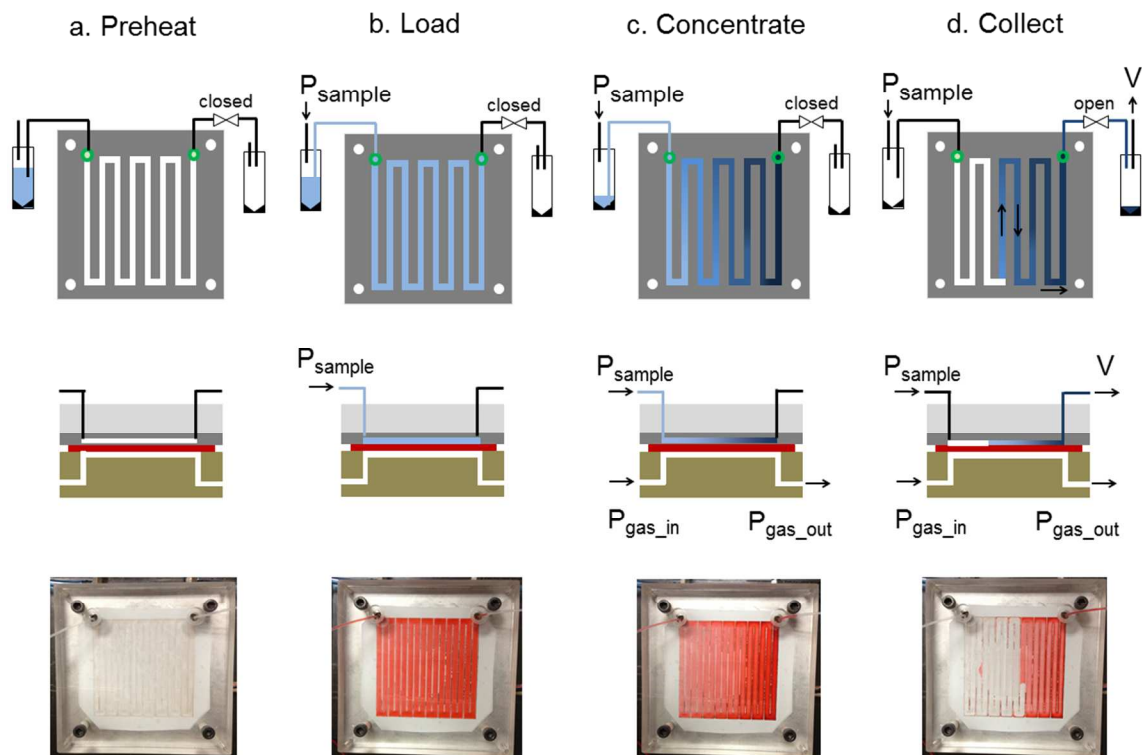
Figure 3. Operation of the microfluidic concentrator. (a) Preheating of the chip to the desired evaporation temperature; (b) Loading of the sample from the reservoir into the chip; (c) Evaporative concentration of the sample to the desired volume; (d) Collection of the concentrated sample from the chip. The top row illustrates a top view schematic of the sample layer of the chip in each step. Darker colors represent more concentrated solutions. The middle row illustrates a side view schematic of the chip to show the pressures applied to the chip during each step. The bottom row shows photographs of the chip during concentration of water containing food dye.
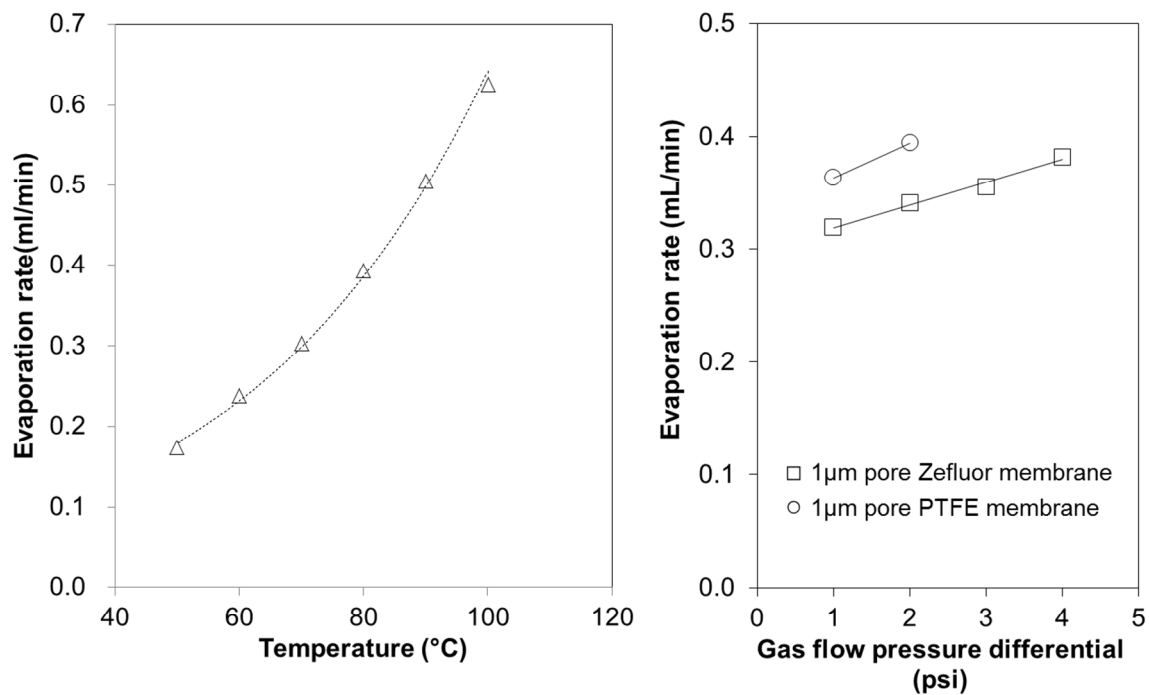
Figure 4: (a) Effect of temperature on the evaporation rate. The 1 µm pore PTFE membrane was used. P_{sample} = 1.5 psig, P_{gas_in} = 1.5 psig, P_{gas_out} = 0.0 psig. (b) Effect of gas flow pressure differential (Pgas_in − Pgas_out) on evaporation rate. P_{sample} = 4.0 psig, P_{gas_out} = 0.0 psig for 1 µm Zefluor membrane and P_{sample} = 2.0 psig, P_{gas_out} = 0.0 psig for 1 µm PTFE membrane. The temperature, T_{chip}, was 80°C for these measurements.
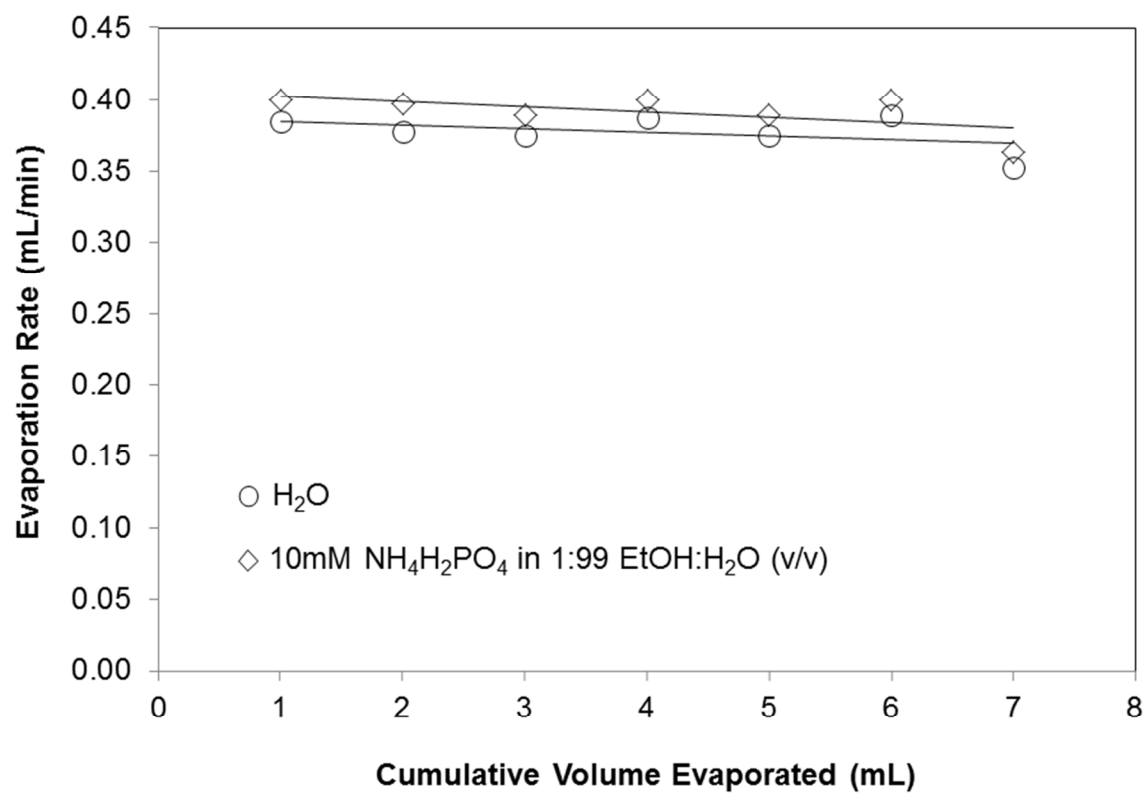
5

Figure 5. Evaporation rate as a function of the amount of solvent volume that has been evaporated
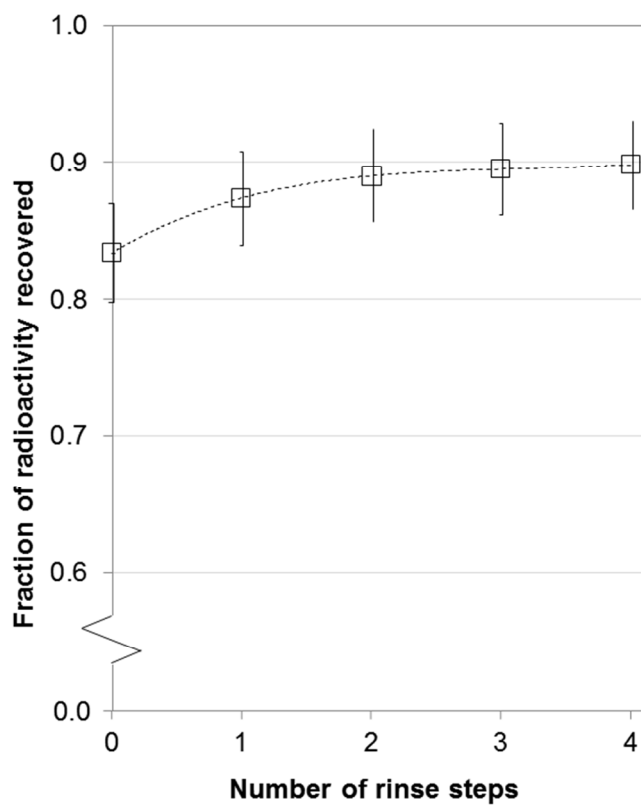
Figure 6. Effect of rinse steps on recovery of the concentrated radioactive sample from the chip. Here, a 10 mL sample of [^{18}F]FDG was concentrated. Data points show the average of three repetitions.

PET tracer		Mobile phase (All ratios are volume:volume)
Common name	Full name	
[18F]FAC	2'-deoxy-2'-[18F]fluoro-β-D-arabinofuranosylcytosine	1:99 EtOH/10mM NH$_4$H$_2$PO$_4$
[18F]FLT	3'-deoxy-3'-[18F]fluoro-L-thymidine	8:92 EtOH/20mM KH$_2$PO$_4$
[18F]FMAU	2'-deoxy-2'-[18F]fluoro-5-methyl-β-L-arabinofuranosyluracil	4:96 EtOH/50mM NH$_4$OA$_C$
[18F]FHBG	9-(4-[18F]fluoro-3-hydroxymethylbutyl)-guanine	5:95 MeCN/50mM NH$_4$OA$_C$
[18F]SFB	N-succinimidyl-4-[18F]fluorobenzoate	50:50 MeCN/water with 0.1% TFA
[18F]Fallypride	(S)-N-[(1-allyl-2-pyrrolidinyl)methyl]-5-(3-[18F]fluoropropyl)-2,3-dimethoxybenzamide	65:45 MeCN/25mM NH$_4$HCO$_2$ with 1%TEA

Table 1. HPLC mobile phases used for purification of several different PET tracers.

5

Convenient, rapid, and repeatable concentration of positron emission tomography (PET) tracers is achieved by microfluidic membrane distillation.